Journal of ELECTRONIC MATERIALS, Vol. 49, No. 2, 2020
https://doi.org/10.1007/s11664-019-07663-z

The Effect of Indium Doping on Deep Level Defects and Electrical Properties of CdZnTe

FAN YANG,[1] WANQI JIE,[1,3] GANGQIANG ZHA,[1] SHOUZHI XI,[2] MIAO WANG,[2] and TAO WANG [1,4]

1.—State Key Laboratory of Solidification Processing, and Key Laboratory of Radiation Detection Materials and Devices, Ministry of Industry and Information Technology, School of Materials Science and Engineering, Northwestern Polytechnical University, Xi'an 710072, Shaanxi, P.R. China. 2.—Imdetek Corporation Ltd, Xi'an 712000, Shaanxi, P.R. China. 3.—e-mail: jwq@nwpu.edu.cn. 4.—e-mail: taowang@nwpu.edu.cn

CdZnTe (CZT) ingots doped with different concentrations of indium (2 ppm, 5 ppm, 8 ppm, and 11 ppm) were grown by the Vertical Bridgman Method. The charge transport behaviors of CZT wafers were characterized by Thermally Stimulated Current (TSC), Time of Flight technique (TOF) and Current–Voltage measurements (*I–V*). TSC results indicate that the concentration of deep donor defects Te_{Cd}^{2+} is reduced significantly by increasing indium dopant content from 2 ppm to 8 ppm, while that of indium related traps, In_{Cd}^{+} and A-centers, is sharply increased. Hecht fitting and TOF results indicate that the electron mobility keeps nearly unchanged for different dopant concentrations in the region between 2 ppm and 5 ppm, but the lifetime increased greatly with increasing indium dopant concentration. Therefore, $(\mu\tau)_e$ value was increased with higher indium dopant. The up-shift of Fermi level is also observed in the temperature-dependent *I–V* result with the increasing of indium dopant content. Large Schottky barriers are found in detectors with higher indium concentration. High voltage x-ray response results show that the channel number shifts to the low energy side for 2 ppm dopant samples compared with best performance 5 ppm dopant samples, while the full-energy peaks are broadened for 8 ppm and 11 ppm dopant samples.

Key words: CdZnTe, indium dopant, deep level defect, electrical property

INTRODUCTION

Single-crystalline cadmium zinc telluride (CZT) has been accepted as the most important room temperature nuclear radiation detection material.[1–3] The high resistivity and high mobility-lifetime product are the key factors for obtaining high signal-to-noise ratio as well as high detection efficiency and resolution.[4] Both of the physical properties are dominated by the point defects, especially cadmium vacancies, which will introduce deep level acceptors and electron traps. Indium doping was proposed to compensate the acceptors and mitigate the negative effects of point defects. The superiorities of indium dopant, such as proper atomic number, high doping efficiency and introducing shallow levels only, are reported.[5,6] However, the quantitative relationship between the dopant concentration and the electrical properties of a crystal are still not clear. The confusing results may also be aroused due to the dopant segregation in Bridgman grown CZT crystal, which means that dopant concentration for the wafers from different positions in the same ingot is quite different.[7–9] Thus, figuring out the underlying impact of indium doping on defects distribution is necessary. Based on the previous researches on the effects of indium dopant,[10,11] we will identify the dominating point

(Received January 2, 2019; accepted September 19, 2019; published online October 18, 2019)

defects in different indium compensated CZT crystals by thermally stimulated current (TSC) spectra. The effects of indium doping content on the concentration of tellurium anti-site, the electron mobility and Fermi level will be discussed, and the energy spectrum will also be analyzed to reveal the effect of the dopant on the detectors' performance.

EXPERIMENTAL

The 7N-purity cadmium, zinc and tellurium in the stoichiometric ratio of $Cd_{0.9}Zn_{0.1}Te$ were used for CZT single crystal growth. We used a high-precision electronic balance with the accuracy of 1×10^{-4} mg to weigh the indium. Indium was added together with the raw material into the synthesis ampoules and sealed under high vacuum of about 3×10^{-5} Pa. The ampoules were then placed into the furnace. After the temperature in the furnace rose upon the CZT melting point, the furnace began the half-circle rocking movement. The furnace kept rocking for more than 24 h and then cooled down. We believe the process is effective to gain uniform polycrystalline ingots. After synthesis, four single-crystalline ingots named CZT1, CZT2, CZT3 and CZT4 with different indium dopant concentrations of 2 ppm, 5 ppm, 8 ppm and 11 ppm (atomic ratio) were grown at Imdetek Corporation. The single-crystalline ingots make the comparison more reliable because the influence of grain boundary is eliminated. The composition distribution in polycrystalline ingots will deviate far from the theoretical mass transfer models. The impurities including the dopant will accumulate in the grain boundaries. Since our work focus on the influence of different indium dopant content, we try to minimize the effect of non-uniform caused by these concerns. The samples were cut from the same region from different single-crystalline ingots, which could be considered having nearly the same component except for indium dopant.

Indium concentration was tested with samples in the size of $2.3 \times 2.3 \times 20$ mm^3 by Glow Discharge Mass Spectrometry (GDMS) in VG 9000 at the National Research Council Canada. The following samples for other tests were cut near the GDMS samples. All electrical property analysis samples were mechanically polished with MgO powder and then chemical-mechanically polished in silica sol suspension, then etched in 5% Br-Methanol for 1 min to remove the surface damaged layer. After the electrodes were deposited, the side surface was passivated in H_2O_2 solution.

The TSC samples have two point electrodes on the same face of the samples with a certain distance. Saturated $AuCl_3$ methanol solution was used to deposit gold electrodes. The diameter of the circular electrodes was about 0.5 mm, and the distance between two electrodes was about 5 mm. TSC measurement was conducted with our homemade equipment. The TSC equipment mainly consists of three parts: low temperature module, light source module and measurement controlling module. The low temperature module includes Sumitomo-202 refrigeration system with the 10 K lowest temperature, Cryoco-M24 temperature controller. The light source module consists of a 75 W halogen lamp and a power supply. The range of the wavelength is 300–2500 nm. The measurement controlling module mainly includes a Keithley-2000 nanovolt meter, a Keithley-2400 voltage supply, and Keithley-6514 *I–V* measurement. The system is fully automatically computer controlled.

Hall measurement was used to confirm the conduction type of the samples. Time of flight (TOF) test was used to obtain electron mobility. Keithley-6517B was utilized to characterize *I–V* curves. The Fermi level of the samples was fitted according to the temperature-dependent *I–V* test results. Planar detectors in the size of $10 \times 10 \times 5$ mm^3 were fabricated with the wafers cut from the same zone of different ingots. The detectors' energy response spectrum under non-collimated ^{241}Am radioactive source was recorded using a homemade system in Imdetek Co., Ltd. Since the energy response test is strongly related with electrical properties, we used it as the comprehensive evaluation on crystal quality.

RESULTS AND DISCUSSION

GDMS results in Table I show the real indium dopant concentrations of the four CZT ingots. The typical TSC curves of the crystals are shown in Fig. 1 where the data is normalized with the area and distance of electrodes. Four peaks can be identified for all the curves.[11] T_1 is considered coming from indium related defects, which increase with the concentration of indium dopant. T_2 and T_3 are from the shallow acceptors of primary ionized cadmium vacancy (V_{Cd}^{-}) and secondary ionized cadmium vacancy (V_{Cd}^{2-}). T_4 is affiliated with Te_{Cd}^{2+}, the major contributor to high resistivity and electron traps.[12–14]

The quantitative trap densities are calculated by applying a multi-Gaussian to fit with the following equation:[15]

$$N_{T_i} = \frac{Q_{T_i}}{2(\mu\tau)_e qAE\beta}, \quad (1)$$

where N_{T_i} and Q_{T_i} are trap density and peak area of peak T_i, respectively. A is the area of the electrode, E is electric field intensity through the sample, β is the heating rate, about 0.2 K/s in this work. We can see that indium related peak T_1 increases sharply with the increasing of dopant content, but the concentrations of T_2 and T_3 related to V_{Cd}^{-} and V_{Cd}^{2-} remain nearly unchanged. The peak T_4 related to deep donor Te_{Cd}^{2+} deceases gradually in the order from CZT1 to CZT3.

Table I. The data of indium content obtained by GDMS and trap densities in CZT samples obtained by peak-differentiation of Fig. 1

Sample	Dopant content (ppm, atomic ratio)	Trap density (cm^{-3})			
		T_1	T_2	T_3	T_4
CZT1	2.2	1.15×10^{13}	6.44×10^{13}	1.76×10^{14}	7.11×10^{13}
CZT2	4.4	5.86×10^{13}	5.42×10^{13}	4.90×10^{13}	9.57×10^{12}
CZT3	7.5	1.03×10^{14}	7.34×10^{13}	2.14×10^{13}	2.19×10^{12}
CZT4	12	2.86×10^{16}	2.27×10^{14}	5.45×10^{13}	2.97×10^{12}

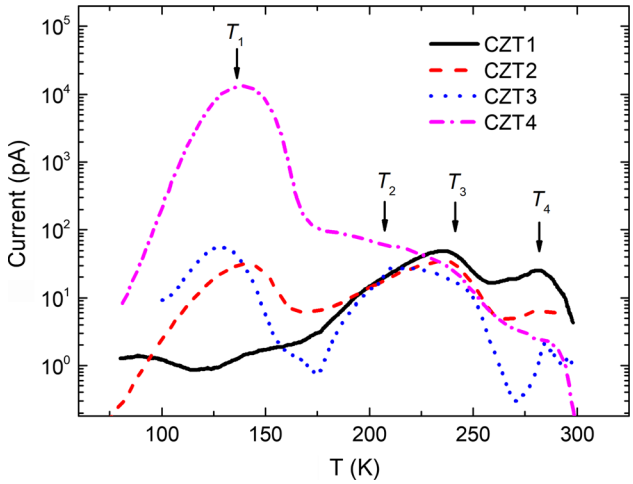

Fig. 1. Typical TSC spectra of 3 mm thickness of CZT samples CZT1 to CZT4.

Considering the possible defect reaction during growth and annealing process,[16]

$$V_{Cd}^{2-} + In \rightarrow In_{Cd}^{+} + 3e^{-}, \quad (2)$$

$$V_{Cd}^{2-} + Te_i \rightarrow Te_{Cd}^{2+} + 4e^{-}, \quad (3)$$

$$In_{Cd}^{+} + V_{Cd}^{2-} \rightarrow \left[In_{Cd}^{+} V_{Cd}^{2-}\right]^{-}, \quad (4)$$

indium dopant occupies cation sites and forms In_{Cd}^{+}. The indium dopant content in CZT1 is quite low so that the concentration of indium related T_1 is very limited. More cadmium vacancies would remain to react with tellurium interstitials. In this case, the concentration of peak T_4 related to deep donor Te_{Cd}^{2+} reaches the same order of magnitude with acceptors V_{Cd}^{-} and V_{Cd}^{2-}. It indicates that the donor–acceptor compensation mainly happened among Te_{Cd}^{2+}, V_{Cd}^{-} and V_{Cd}^{2-}. As the indium dopant content increases, excess of cadmium vacancies decreases, and therefore Te_{Cd}^{2+} reduces. In CZT2, the concentration of T_1 is at the same level as T_2 and T_3 while T_4 is lowered by one order of magnitude. It means the shallow donors and acceptors were properly compensated. When we further increase the dopant content, the remaining cadmium vacancies became very limited and the density of Te_{Cd}^{2+} kept almost unchanged. Moreover, the density of T_1 reaches 2.86×10^{16} cm^{-3} in CZT4, which is extremely excessive over T_2 and T_3. Considering that the resistivity is still as high as 6.3×10^9 Ω cm (Table II), T_1 could not be attributed by In_{Cd}^{+} alone. We suppose that the complex $\left[In_{Cd}^{+} V_{Cd}^{2-}\right]^{-}$ (about 0.14 eV under conduction band) formed, which was explained as self-compensation.[17]

The basic photoelectric properties of the four crystals are shown in Table II. Although the indium content varies from 2 ppm to 11 ppm, the resistivity of four samples is all above 5×10^9 Ω cm. The mobility-lifetime products were fitted with modified Hecht equation.[18] The $(\mu\tau)_e$ value of CZT1 is significantly lower than those of CZT2 to CZT4.

Figure 2 shows TOF results of CZT1 and CZT2. Those of CZT3 and CZT4 are nearly the same as CZT2. Dropping down of the signals in the initial stage is attributed to surface recombination. The transition time T_R is obtained from the endpoint of the transition platform and utilized to estimate electron drift velocity.[19] The slope of linear fitting on electric field versus velocity reveals the electron mobility. According to Fig. 2b and d the mobility of CZT1 is 1173 cm^2/Vs, which is close to the value of 1118 cm^2/Vs for CZT2. Combining mobility in Fig. 2 and electron $\mu\tau$ values in Table II, the lifetimes of CZT1 and CZT2 are about 750 ns and 1450 ns, respectively. The excess of Te_{Cd}^{2+} may be responsible for the short electron lifetime of CZT1.[20]

The Fermi level position is measured by temperature-dependent *I–V* test, which can be deduced by the following equation:[21]

$$\frac{E_F - E_c}{kT} = \ln I + C. \quad (5)$$

where E_c and E_F stand for energy level position of conduction band edge and Fermi level, respectively, I is the current between the electrodes at corresponding temperature T, C is constant independent of temperature, and k is the Boltzmann constant. It should be mentioned that the Fermi level is temperature-dependent, and shifts down to the middle of the forbidden band as the temperature become higher in *n*-type semiconductors. Here in our

Table II. Basic photoelectric properties for the crystals from the four ingots

Sample	Resistivity (Ω cm)	Conduction type	$(\mu\tau)_e$ (cm^2/V)
CZT1	1.67×10^{10}	n	0.88×10^{-3}
CZT2	1.32×10^{10}	n	1.62×10^{-3}
CZT3	0.96×10^{10}	n	1.47×10^{-3}
CZT4	0.63×10^{10}	n	1.28×10^{-3}

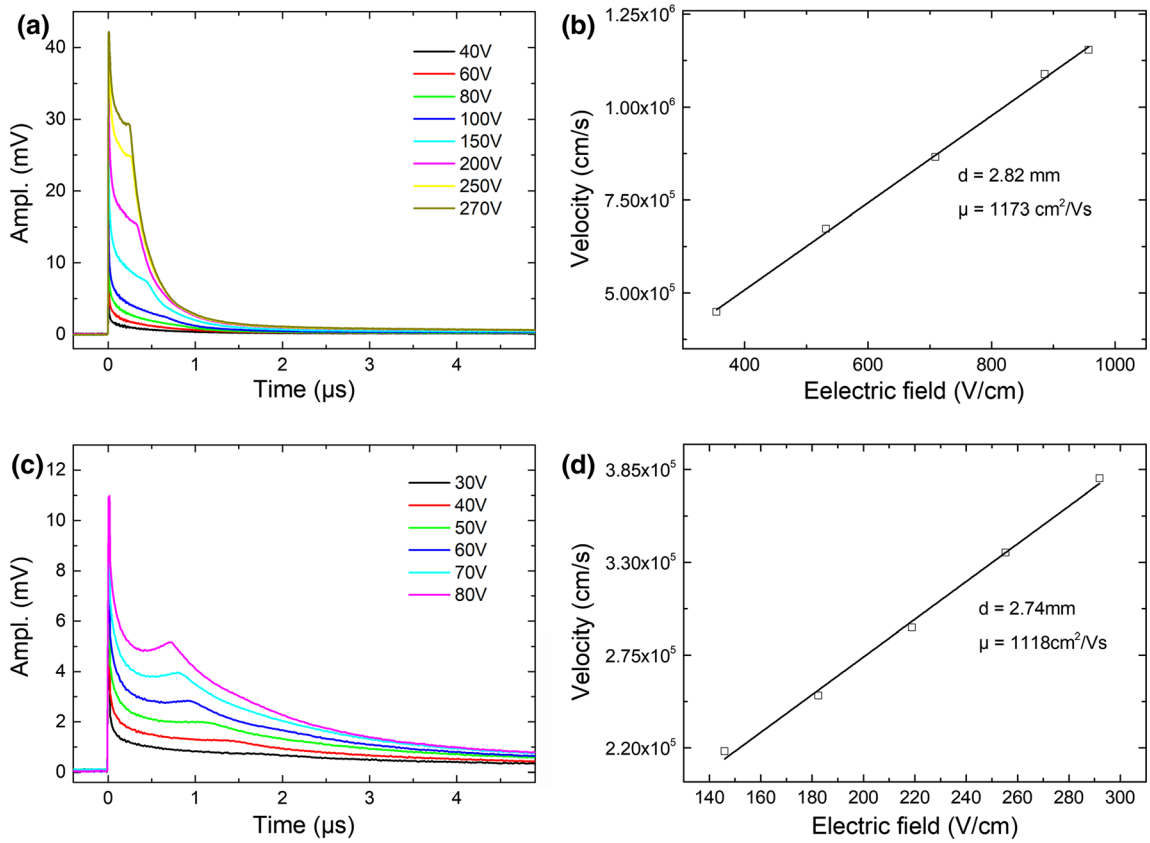

Fig. 2. TOF curves under different bias voltages. (a) and (c) TOF curves under different bias voltages of samples CZT1 and CZT2, (b) and (d) linear fitting of electric field versus velocity and the calculated mobility of samples CZT1 and CZT2.

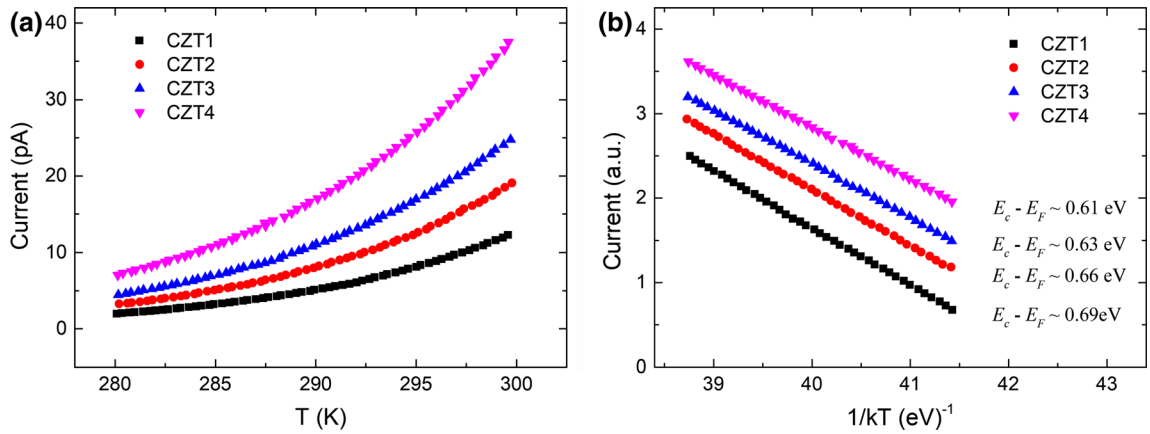

Fig. 3. Results of temperature dependent *I–V* test. (a) The current versus temperature, (b) linear fitting results of $1/(kT)$ and ln*I*.

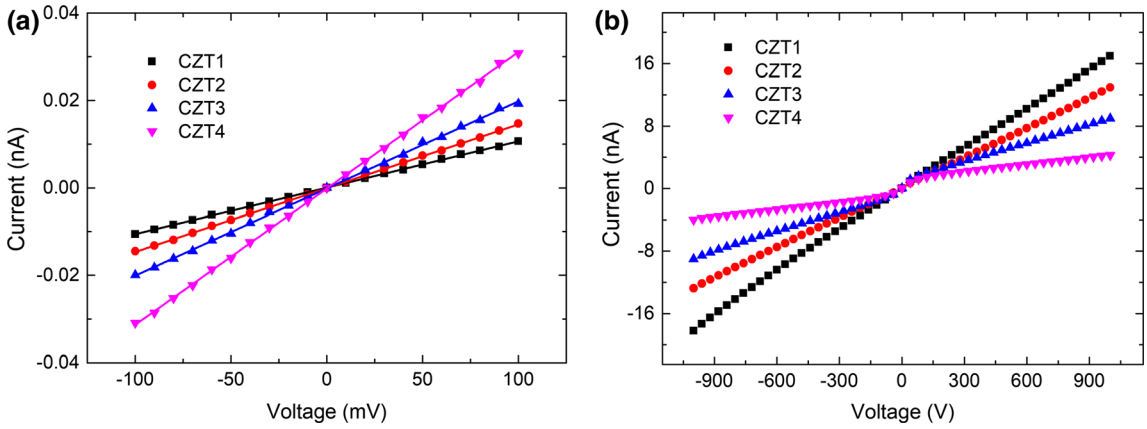

Fig. 4. Current–voltage curves of the samples CZT1 to CZT4. (a) The bias ranges from − 0.1 V to 0.1 V, (b) the bias ranges from − 1000 V to 1000 V.

experiment, the temperature variation is only about 20 K and can be neglected.

According to temperature-dependent I–V results, the linear fitting curves of $1/(kT)$ and $\ln I$ for samples CZT1 to CZT4 are shown in Fig. 3. The difference between conduction band edge and Fermi level ($E_c - E_F$) was deduced to be 0.69 eV to 0.61 eV for CZT1 to CZT4. As the band gap of CdZnTe is about 1.5–1.6 eV,[21] the Fermi level shifts up about 0.08 eV along with indium dopant content increases from 2 ppm to 11 ppm. This should be the major reason for resistivity decline for samples CZT1 to CZT4 in Table II. As we know, donor dopant in a semiconductor will pull Fermi level to the direction of the conduction band. Furthermore, the effect of Fermi level pinning caused by tellurium anti-site is widely accepted as the major reason for the high resistivity of CZT crystals.[20,22] In our study the pinning effect may be faded since the density of tellurium anti-site was limited by excessive indium dopant.

Samples in the dimension of $10 \times 10 \times 5$ mm^3 were fabricated into parallel plane detectors. After the electrodes were deposited on the crystal surface, and further protected by photoresist before putting the detectors in H_2O_2 solution for passivation to suppress the side surface leakage current. The resistivity under the bias of 0.1 V was estimated according to Fig. 4a. The high bias I–V curve is plotted in Fig. 4b, where I–V curves of CZT3 and CZT4 are S-type, dependent on the contact barrier.[23] Except for resistivity difference, the work function decrease is another result caused by Fermi level shifting up. As a result, the Schottky barrier at the interface between n-type CZT and gold electrode increased. In this situation, the increased dopant content led to larger contact barrier and lower resistivity.

Typical energy spectrums under non-collimated ^{241}Am γ-source with a characteristic energy of 59.5 keV are exhibited in Fig. 5. The collection time for all the detectors is the same of about 60 s. The

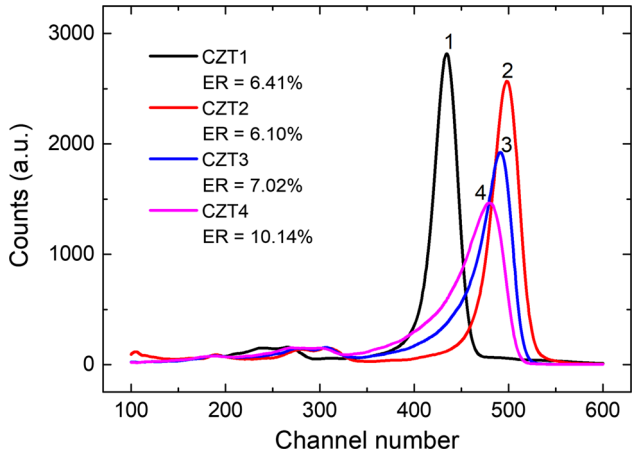

Fig. 5. Radiation response spectrum under ^{241}Am γ-source measured with the applied bias of 1000 V.

total count of the full energy peak is larger than 10 k. The 5 mm thick detectors are tested under 1000 V bias. Compared to the other three detectors, CZT1 has a lower full-energy peak channel number, which indicates the incomplete collection of electrons. According to short electron lifetimes in CZT1, electron trapping during the drift process is more serious, from which the charge collection on the electrodes was reduced. For samples CZT2 to CZT4, the channel number decrease is not obvious while the energy resolution deteriorates seriously from 6.1% to 10.14%. We attribute the peak broadening to a large Schottky barrier. In the barrier depletion region, ionization probabilities of deep levels will be increased.[24] Furthermore, the space charge built by contact barrier will distort the electric field. These factors are considered to be detrimental to charge collection and thus broaden the peak.[25]

CONCLUSION

We have grown four single-crystalline $C_{0.9}Z_{0.1}Te$ ingots by modified the Vertical Bridgman Method with different indium dopant content of 2 ppm,

5 ppm, 8 ppm and 11 ppm, named CZT1, CZT2, CZT3 and CZT4. The defect concentrations obtained from TSC measurement show that from CZT1 to CZT4 the concentration of indium related defect increases from 10^{13} cm^{-3} to 10^{16} cm^{-3}, while the tellurium anti-site decreases from 10^{13} cm^{-3} to 10^{12} cm^{-3}. The densities of cadmium vacancies are about 2×10^{13} cm^{-3} to 2×10^{14} cm^{-3} for all the samples. Through Hecht fitting and TOF results, CZT1 with lower indium content shows a shorter lifetime compared with the other three samples with higher indium dopant concentrations. The difference between conduction band edge and Fermi level reduces from 0.69 eV to 0.61 eV from CZT1 to CZT4, which is considered as the reason for the increase of resistivity from samples CZT1 to CZT4. In x-ray response spectra, CZT1 has lower peak channel number than others due to its low $(\mu\tau)_e$ value, while the gradual half-peak width expansion from CZT2 to CZT4 are supposed to be related to their contact barrier enlargement.

ACKNOWLEDGMENTS

This work was supported by the National Natural Science Foundation of China (51672216), the National Key R&D Program of China (2016YFB0402405, 2016YFF0101301), the Fundamental Research Funds for the Central Universities (3102019ghxm015), and the Research Fund of the State Key Laboratory of Solidification Processing (NPU), China (Grant No. 2019-TS-05).

REFERENCES

1. Y. Eisen and A. Shor, *J. Cryst. Growth* 184–185, 1302 (1998).
2. T.E. Schlesinger, J.E. Toney, H. Yoon, E.Y. Lee, B.A. Brunett, L. Franks, and R.B. James, *Mater. Sci. Eng. R: Rep.* 32, 103 (2001).
3. V.M. Zaletin, *At. Energy* 97, 773 (2004).
4. V.M. Azhazha, V.E. Kutnii, A.V. Rybka, I.N. Shlyakhov, D.V. Kutnii, and A.A. Zakharchenko, *At. Energy* 92, 508 (2002).
5. R. Gul, K. Keeter, R. Rodriguez, A.E. Bolotnikov, A. Hossain, G.S. Camarda, K.H. Kim, G. Yang, Y. Cui, V. Carcelén, J. Franc, Z. Li, and R.B. James, *J. Electron. Mater.* 41, 488 (2012).
6. M. Fiederle, A. Fauler, J. Konrath, V. Babentsov, J. Franc, and, R.B. James, *IEEE Trans. Nucl. Sci.* 51, 1864 (2004).
7. O. Panchuk, A. Savitskiy, P. Fochuk, Y. Nykonyuk, O. Parfenyuk, L. Shcherbak, M. IIashchuk, L. Yatsunyk, and P. Feychuk, *J. Cryst. Growth* 197, 607 (1999).
8. M.R. Lorenz, *J. Phys. Chem. Solids* 23, 939 (1962).
9. E. Watson and D. Shaw, *J. Phys. C: Solid State Phys.* 16, 515 (1983).
10. G. Yang, W. Jie, Q. Li, T. Wang, G. Li, and H. Hua, *J. Cryst. Growth* 283, 431 (2005).
11. L. Xu, W. Jie, X. Fu, A.E. Bolotnikov, R.B. James, T. Feng, G. Zha, T. Wang, Y. Xu, and Y. Zaman, *J. Cryst. Growth* 409, 71 (2015).
12. M. Chu, S. Terterian, D. Ting, C.C. Wang, H.K. Gurgenian, and S. Mesropian, *Appl. Phys. Lett.* 79, 2728 (2001).
13. M. Fiederle, C. Eiche, M. Salk, R. Schwarz, and K.W. Benz, *J. Appl. Phys.* 84, 6689 (1998).
14. V. Babentsov, J. Franc, P. Hoeschl, M. Fiederle, K. Benz, N. Sochinskii, E. Dieguez, and R. James, *Cryst. Res. Technol.* 44, 1054 (2009).
15. M. Pavlović and U.V. Desnica, *J. Appl. Phys.* 84, 2018 (1998).
16. Q. Li, W. Jie, L. Fu, T. Wang, G. Yang, X. Bai, and G. Zha, *J. Cryst. Growth* 295, 124 (2006).
17. L. Shcherbak, P. Feychuk, O. Kopach, O. Falenchuk, and O. Panchuk, *J. Chim. Phys.* 95, 1757 (1998).
18. J.P. Biersack and L.G. Haggmark, *Nucl. Instrum. Methods* 174, 257 (1980).
19. J.C. Erickson, H.W. Yao, R.B. James, H. Hermon, and M. Greaves, *J. Electron. Mater.* 29, 699 (2000).
20. G. Zha, J. Yang, L. Xu, T. Feng, N. Wang, and W. Jie, *J. Appl. Phys.* 115, 043715 (2014).
21. Y. Xu, W. Jie, P. Sellin, T. Wang, W. Liu, G. Zha, P. Veeramani, and C. Mills, *J. Phys. D Appl. Phys.* 42, 035105 (2009).
22. T. Takahashi, and S. Watanabe, *IEEE Trans. Nucl. Sci.* 48, 950 (2001).
23. A.E. Bolotnikov, S.E. Boggs, C.M.H. Chen, W.R. Cook, and F.A. Harrison, SM Schindler. *Nucl. Instrum. Methods Phys. Res. Sect. A* 482, 395 (2002).
24. A. Cola and I. Farella, *Appl. Phys. Lett.* 105, 203501 (2014).
25. Z. He, G.F. Knoll, D.K. Wehe, and J. Miyamoto, *Nucl. Instrum. Methods Phys. Res. Sect. A* 388, 180 (1997).